Fluid Dynamics & Materials Processing

Tech Science Press

DOI: 10.32604/fdmp.2023.025966

ARTICLE

Research on the Corrosion of J55 Steel Due to Oxygen-Reducing Air Flooding in Low-Permeability Reservoirs

Liang Wang[1], Baofeng Hou[1], Yanming Fang[3], Jintao Zhang[2] and Fajian Nie[1,2,*]

[1]School of Petroleum Engineering, Yangtze University, Wuhan, 430100, China

[2]Beijing Huacheng Hengye Petroleum Technology Development Limited Company, Beijing, 101499, China

[3]Petroleum Engineering Technology Research Institute of North China Oil & Gas Company, Zhengzhou, 450006, China

[*]Corresponding Author: Fajian Nie. Email: niefajian@163.com

Received: 08 August 2022 Accepted: 25 October 2022

ABSTRACT

Oxygen-reducing air flooding is a low-permeability reservoir recovery technology with safety and low-cost advantages. However, in the process of air injection and drive, carbon in the air is oxidized through the crude oil reservoir to generate CO_2, and this can cause serious corrosion in the recovery well. In this study, experiments on the corrosion of J55 tubular steel in a fluid environment with coexisting O_2 and CO_2 in an autoclave are presented. In particular, a weight loss method and a 3D morphometer were used to determine the average and the local corrosion rate. The corrosion surface morphology and composition were also measured by means of scanning electron microscopy (SEM) and an X-ray diffractometer (XRD). The corrosion pattern and morphological characteristics of J55 steel were analyzed in the O_2/CO_2 environment for different degrees of oxygen-reduction. As made evident by the experimental results, the corrosion products were mainly ferrous carbonate and iron oxide. In general, air injection increases the degree of oxygen reduction, from oxygen corrosion characteristics to CO_2 corrosion-based characteristics. As a result, the corrosion product film becomes denser, and the corrosion rate is lower.

KEYWORDS

J55 steel; O_2/CO_2 corrosion; corrosion product film; oxygen-reducing air flooding

1 Introduction

Oxygen-reduced air flooding is a low-risk and low-cost tertiary oil recovery technology that has recently emerged. The mechanism of air flooding is to make the oxygen in the air react with the crude oil by low-temperature oxidation. It generates CO and CO_2 while regulating the viscosity of crude oil and then combines with N_2 and light hydrocarbon components to form flue gas to repel crude oil [1,2]. For low-permeability reservoirs, if un-reduced-oxygen air is injected directly for oil flooding, the oxygen in the injected gas does not enter the reservoir in time, leading to a high oxygen concentration in the production wells, which may heighten the risk of explosion [3,4]. Therefore, the method of reducing the oxygen content in the air to a pre-determined level by air separation equipment before injection has received wide attention. Oil fields such as Changqing, Qinghai, and North China have started to apply oxygen-reducing air flooding to the extraction of low-permeability oil fields.

In the process of air injection and oil flooding, the oxygen in the air reacts with the reservoir crude oil to produce CO_2, and the O_2 and CO_2 together cause corrosion to the tubular column in the extraction section [5–7], resulting in serious deterioration of the tubular column in the extraction well. It affects the safety of oil well extraction and causes huge economic losses. The current research on J55 steel mainly involves corrosion in a single gas (O_2 or CO_2) environment. The O_2 and/or CO_2 in the air or neutral solution, and the mechanism of electrochemical corrosion are shown in Fig. 1. Zhu concluded that in an environment of O_2 and CO_2 coexistence, the corrosion product film on the material surface does not form a dense protective layer, and the synergistic corrosion effect of O_2 and CO_2 is stronger than the single corrosion effect of O_2 or CO_2 only [8]. Zhang et al. [9] argued that the corrosion products produced under the synergistic corrosion of O_2 and CO_2 have less adhesion to the metal surface, are easy to fall off, and the corrosion rate is significantly greater than the corrosion rate of O_2 and CO_2 under a single component. At the same time, the main product of the corrosion reaction is produced under high-temperature conditions. $FeCO_3$ is more stable and has good film-forming properties. And oxidation generated by Fe_2O_3 and FeOOH protection is weak [10–12].

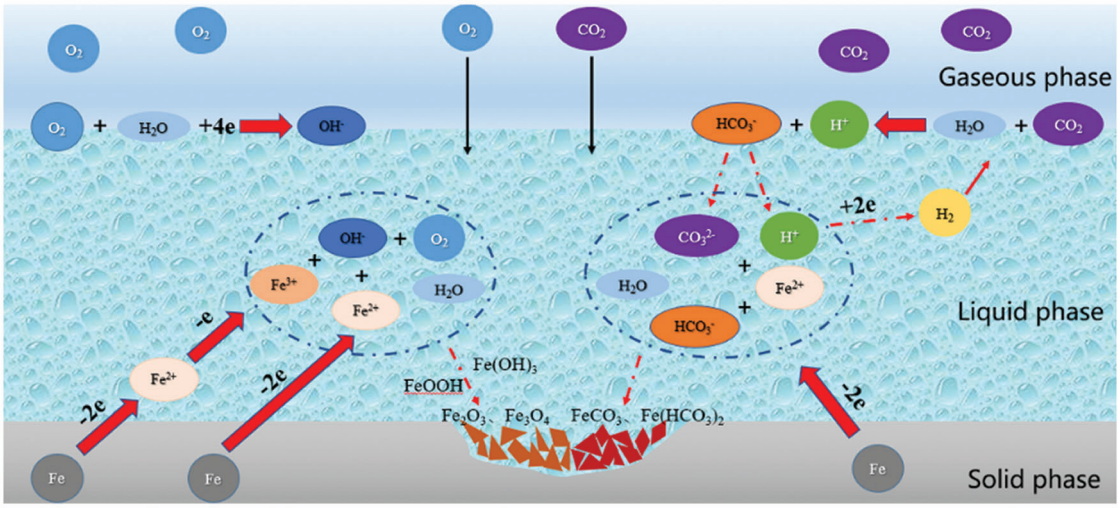

Figure 1: Schematic diagram of the electrochemical corrosion process of O_2 and CO_2

As shown in Fig. 2, the oxygen concentration of oxygen-reduced air is less costly when it is between 6% and 10%. The cost difference between 6% and 10% is not significant. In this paper, three groups of oxygen-reduced air with 6%, 8% and 10% oxygen concentrations were selected. The O_2 and CO_2 partial pressures after injection into the corresponding output wells through reservoir oxidation were simulated. Corrosion experiments were conducted on J55 steel in a hot fluid environment. Corrosion experiments of J55 steel were conducted in a single O_2 and CO_2 environment for control.

2 Experimental Methods

2.1 Experimental Materials

Corrosion pegs: J55 steel, size 72.4 mm × 21.5 mm × 2.2 mm. The chemical composition of the J55 steel used is shown in Table 1.

Corrosion solution: simulated groundwater. The simulated formation water used in this experiment was formulated with reference to the field formation water components, and the component concentrations of the simulated formation water are presented in Tables 2 and 3.

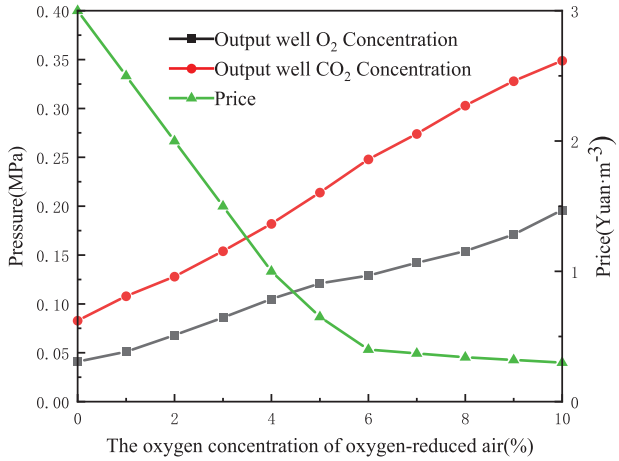

Figure 2: Price of oxygen-reduced air production with different oxygen content and O_2 and CO_2 partial pressure in the output well after injection [2]

Table 1: J55 steel chemical composition (Mass percent)

C	P	S	Si	Cr	Mn	Mo	Ni	Cu	Fe
0.324%	0.015%	0.017%	0.226%	0.049%	1.544%	0.007%	0.026%	0.020%	Residuals

Table 2: Simulated groundwater component concentrations (pH = 5.3)

Components	Content (mg/L)
K^+, Na^+	21404
Ca^{2+}	5480
Mg^{2+}	1464
Cl^-	38198
HCO_3^-	183
SO_4^{2-}	672

Table 3: O_2 and CO_2 partial pressures corresponding to different corrosion experiments (total pressure 3 MPa)

	O_2 partial pressure (MPa)	CO_2 partial pressure (MPa)
10% oxygen concentration minus oxygen air	0.2	0.35
8% oxygen concentration minus oxygen air	0.16	0.30
6% oxygen concentration minus oxygen air	0.12	0.25
Pure O_2	0.2	0
	0.16	0
	0.12	0
Pure CO_2	0	0.35
	0	0.30
	0	0.25

2.2 Experimental Equipment

The equipment used in this experiment are a high-temperature autoclave (Hastelloy high-temperature and high-pressure corrosion system: volume 10 L, maximum working pressure 10 MPa, maximum working temperature 240°C); HH-8 digital display constant temperature water bath; JJ-1 magnetic heating stirrer; JJ223BC electronic precision balance; 5W-W electric, desktop, regular temperature drying oven, JSM-6390 scanning electron microscope; XRD-6000 diffractometer; CoutourGT-X three-dimensional morphology instrument.

2.3 Experimental Conditions

Temperature: 60°C, speed: 150 r/min, corrosion time: 7 days.

2.4 Experimental Steps

Each group of experiments consisted of three parallel specimens (I, II, III). Specimen I is used to test the surface morphology and corrosion product composition. Specimen II tests the three-dimensional morphology and local corrosion rate after the film removal. Specimens II, III push the uniform corrosion rate after removing film and takes the average value. Experiment-specific operation steps [13–17] are as follows:

(1) Firstly, the pegs were polished and sanded to the same degree of finish on their surfaces, corners, and holes. Then rinsed with deionized water and put into acetone to degrease. Then soaked in anhydrous ethanol to further degrease and dehydrate. Finally, the pegs were dried, measured, and weighed.

(2) Fig. 3 shows the schematic diagram of the high-temperature and high-pressure corrosion experimental device.

(3) Set the speed of the reactor, raise the temperature to the preset temperature (60°C), and wait for the temperature to stabilize. Pass in N_2 to replenish the pressure in the kettle to 3 MPa. Start the corrosion experiment, remove the hanging piece after seven days, and observe and record the surface condition before treatment.

(4) Specimen I was placed in a drying dish after rinsing, dehydration, and cold air drying, and then the microscopic morphology of corrosion products was observed by scanning electron microscopy. Next, the film composition of corrosion products was analyzed by XRD diffractometer.

(5) Specimens II and III, another set of empty pegs, were put into the ultrasonic cleaning machine containing hydrochloric acid washing solution to remove corrosion products. The ratios of the pickling solution are as follows: 35 mL hydrochloric acid (37% concentration). 315 mL pure water and 3.15 g hexamethyltetramine. The cleaning temperature is 30°C, with a cleaning time of 15 min. After the completion of acid cleaning, the hanging piece was subjected to anhydrous ethanol dehydration, and then put in the drying oven for one h. At the end of oven-drying, the pegs were taken out, weighed, and the average corrosion rate calculated as shown below:

$$V = \frac{8.76 \times 10^4 \times [(m_1 - m_2) - (m_3 - m_4)]}{S \times t \times \rho} \tag{1}$$

where: V is the uniform corrosion rate, mm/a; m_1 is the mass of the hanging piece before cleaning g; m_2 is the mass of the hanging piece after cleaning, g; m_3 is the mass of the blank hanging piece before cleaning, g; m_4 is the mass of the blank hanging piece after cleaning, g; S is the surface area of the test piece, cm^2; t is the the experimental time, h; ρ is the material density of the hanging piece, g/cm^3.

(6) After weighing specimen II, the three-dimensional morphology instrument was used to observe the three-dimensional morphology of the hanging sheet after the removal of corrosion products, and the local corrosion rate was calculated as follows:

$$V' = \frac{\Delta h}{t} \tag{2}$$

where: V' is the local corrosion rate, Δh is the corrosion pit depth, t is the hanging corrosion time.

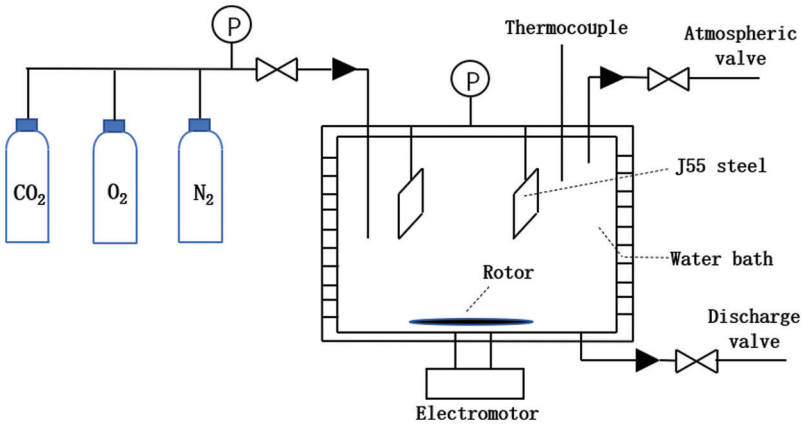

Figure 3: High-temperature and high-pressure dynamic hanging corrosion experimental device schematic diagram

3 Experimental Results and Discussion

3.1 Corrosion Morphological Characteristics

Fig. 4 shows the corrosion morphology of J55 steel under the fluid environment of a single O_2/CO_2 corrosive medium, respectively. As seen in Fig. 4a, the corrosion products on the surface of the specimen in a single O_2 environment (O_2 partial pressure of 0.2 MPa) are dark brown. The surface of the peg is distributed with uneven pitting, and its microscopic morphology shows obvious cracks and pores. Fig. 4b shows that the specimen surface corrosion layer is thin and relatively flat in a single CO_2 environment (CO_2 partial pressure of 0.35 MPa). SEM observations show that the corrosion product is a dense accumulation of blocks. Corrosion product film has a certain protective effect on the metal matrix.

Fig. 5 shows the macroscopic morphology and microscopic morphology of corrosion of J55 steel under three groups of O_2 and CO_2 mixed gas environments with different partial pressures. It is observed that there are corrosion products stacked on the material surface in all groups of environments. But in different O_2/CO_2 partial pressure environments, the type of corrosion layer and degree of corrosion differ. As shown in Fig. 5a, the corrosion products are thicker and looser in the O_2 partial pressure of 0. 2 MPa and CO_2 partial pressure of 0.35 Mpa than what was seen in the single O_2 (O_2 partial pressure of 0.2 MPa) environment. Cracks and pores are more obvious. There is an obvious corrosion layer-off phenomenon in the microscopic morphology of the point pit at the attachment of fine white grains. SEM observations showed that the cracks have a large leaf-like corrosion material generated. In O_2 partial pressure of 0.16 MPa, and CO_2 partial pressure of 0.3 MPa, the corrosion layer is thin, and the corrosion layer appears dark brown. This indicates that the degree of corrosion of the specimen is slowed down. Through the microscopic morphology, it was observed that the corrosion layer still has some voids, while the inner layer of blade-like corrosion products is denser. In the O_2 partial pressure of 0.12 MPa and CO_2 partial pressure of 0.25 MPa, the corrosion layer is flatter and thicker, with no obvious local corrosion pits. SEM observations show that the corrosion products on the metal surface were a dense accumulation of blocks, indicating that the characteristic CO_2 corrosion dominated [18–20]. The above morphological features of corrosion indicate that the decline of J55 steel under the synergistic effect of O_2 and CO_2 is more serious than in single O_2 or CO_2 environment. The corrosion situation is significantly reduced by the injection of increasingly oxygen-reduced air.

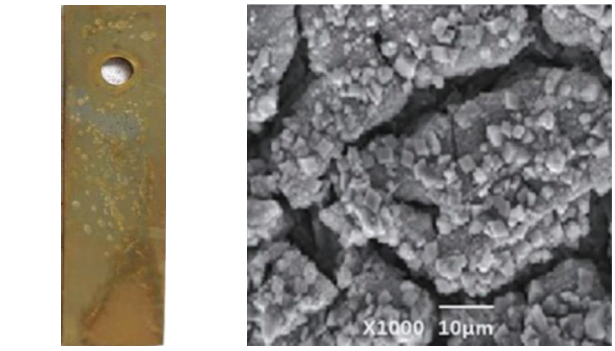

Macroscopic morphology SEM microscopic morphology

(a) Single O_2 (0.2 MPa)

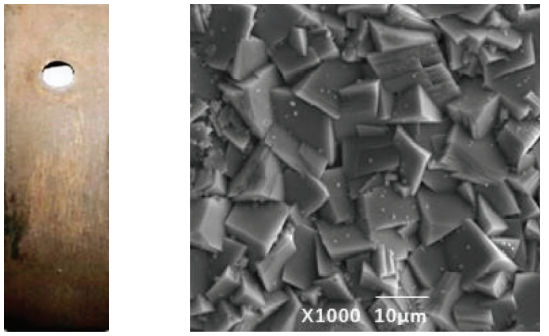

Macroscopic morphology SEM microscopic morphology

(b) Single CO_2 (0.35 MPa)

Figure 4: Corrosion profile of J55 steel in a single O_2/CO_2 environment

3.2 Analysis of the Composition of Corrosion Product Films

From Fig. 6a, the corrosion product film of J55 steel in a single O_2 environment (O_2 partial pressure of 0.2 MPa) was mainly composed of iron oxide. It showed irregular distribution characteristics on the metal surface. And a small amount of Fe elements was detected on the corrosion product film surface. It indicates that the morphology of the corrosion product film in some areas of the single O_2 environment is very thin, leading to the detection of the inner metal composition by X-ray breakdown of the corrosion product film [21]. From Fig. 6b, in a single CO_2 environment (CO_2 partial pressure of 0.35 MPa), the corrosion product film of J55 steel is mainly composed of ferrous carbonate and a small amount of $Fe(HCO_3)_2$.

In the coexistence of O_2 and CO_2, the main products of corrosion are $FeCO_3$ and Fe oxides (Fe_2O_3 is dominant), as determined from the XRD pattern analysis. As shown in Fig. 7a, the supersaturation of Fe^{2+} and CO_3^{2-} in the solution is larger when the partial pressure of O_2 is 0. 2 MPa and the partial pressure of CO_2 is 0.35 MPa. The grain nucleation rate is higher this time, and the $FeCO_3$ grains formed are relatively small. The white grains generated in Fig. 5a are $FeCO_3$, and trace amounts of Fe_3O_4 and FeOCl are also generated due to the high concentration of dissolved oxygen in the solution. However, the peak value of $FeCO_3$ increases with the decrease of CO_2 concentration, and Fe_3O_4 is no longer produced. As shown in Fig. 7c, the peak value of $FeCO_3$ tends to be constant when the partial pressure of O_2 is 0.12 MPa, and the partial pressure of CO_2 is 0.25 MPa, while the amount of Fe_2O_3 production decreases significantly. When the oxygen concentration and CO_2 concentration are reduced simultaneously, the amount of $FeCO_3$ on the steel surface increases. The $FeCO_3$ corrosion product film is denser, which can alleviate the oxygen-induced corrosion effect on the J55 steel sheet [22]. According to XRD analysis, the main corrosion reaction processes of J55 steel in different corrosive media are as follows [23–28].

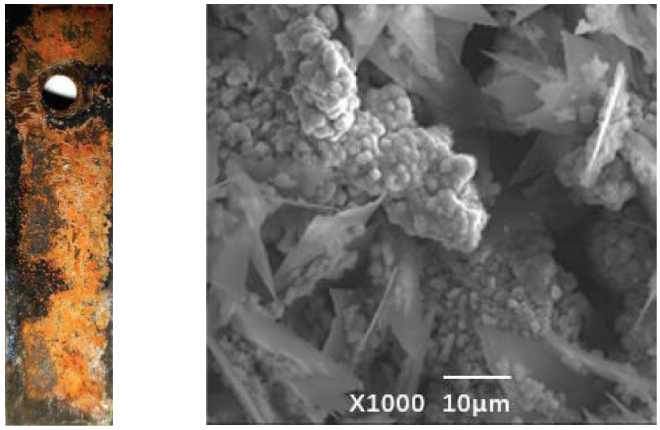

Macroscopic morphology SEM microscopic morphology

(a) O_2 partial pressure of 0.2MPa and CO_2 partial pressure of 0.35MPa (10% oxygen-concentration air flooding production well)

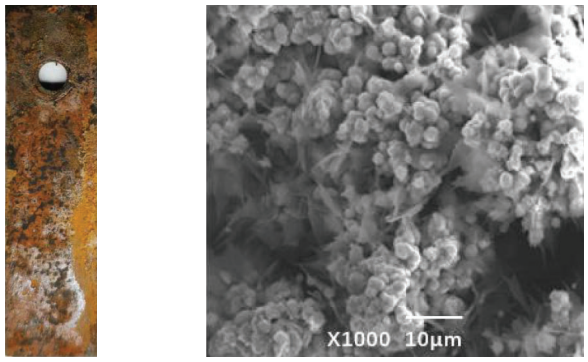

Macroscopic morphology SEM microscopic morphology

(b) O_2 partial pressure of 0.16MPa and CO_2 partial pressure of 0.3MPa (8% oxygen-concentration air flooding production well)

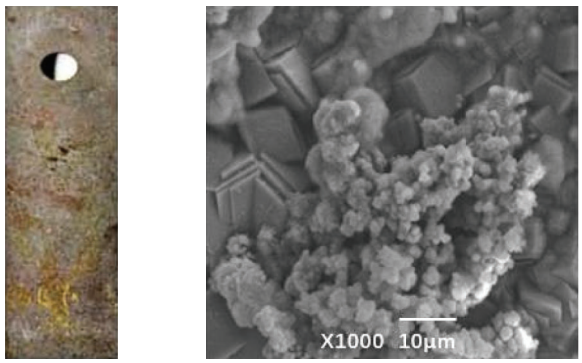

Macroscopic morphology SEM microscopic morphology

(c) O_2 partial pressure of 0.12MPa and CO_2 partial pressure of 0.25MPa (6% oxygen-concentration air flooding production well)

Figure 5: Macroscopic appearance of J55 steel corrosion under different partial pressure O_2/CO_2 coexistence environment

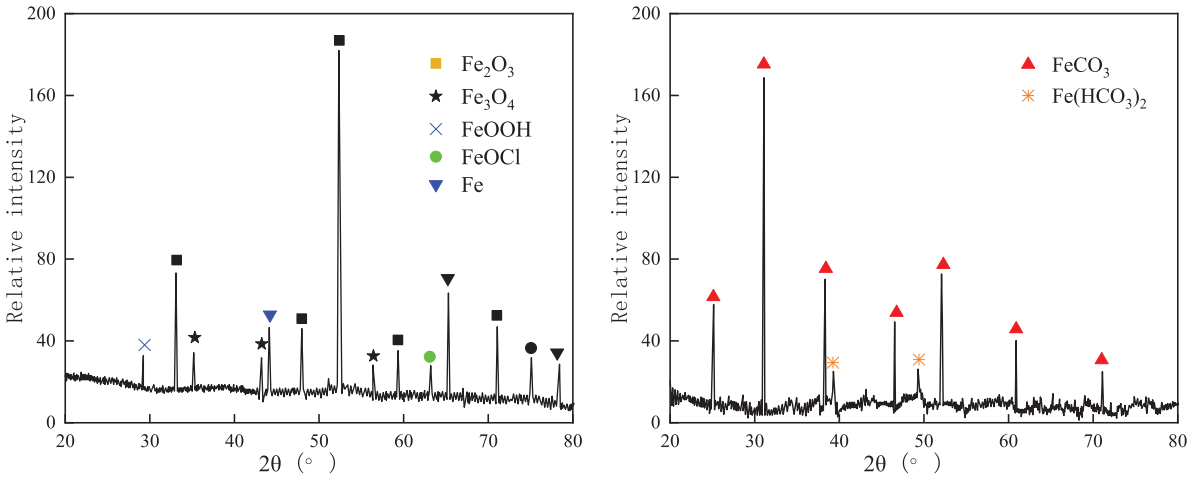

(a) Single O_2 (0.2 MPa) (b) Single CO_2 (0.35 MPa)

Figure 6: XRD pattern of corrosion products of J55 steel in a single O_2/CO_2 environment

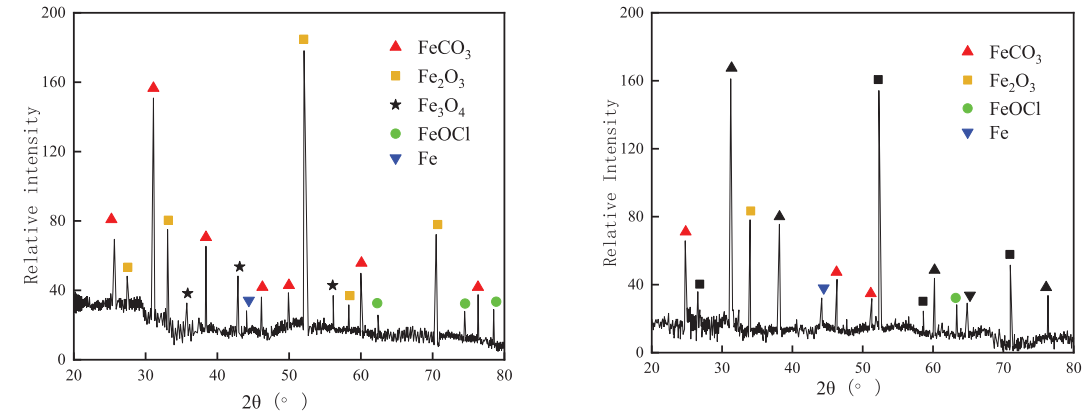

(a) O_2 partial pressure 0.2MPa, CO_2 partial pressure 0.35MPa (10% oxygen-concentration air flooding production well)

(b) O_2 partial pressure 0.16MPa, CO_2 partial pressure 0.3MPa (8% oxygen-concentration air flooding production well)

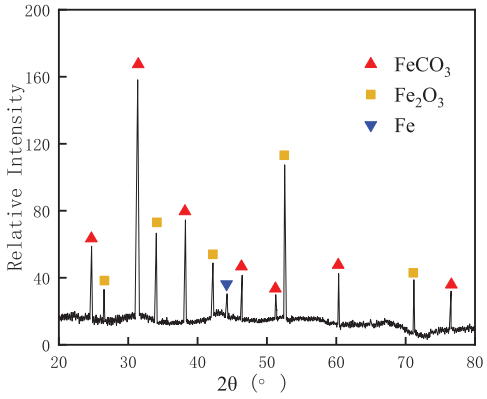

(c) O_2 partial pressure 0.12MPa, CO_2 partial pressure 0.25MPa (6% oxygen-concentration air flooding production well)

Figure 7: XRD pattern of corrosion products of J55 steel under the coexistence of O_2 and CO_2

(1) Reaction under the action of CO_2

Anodic reaction:

$$Fe \rightarrow Fe^{2+}+2e \tag{3}$$

Cathodic reaction:

$$CO_2 + H_2O \rightarrow H^+ + HCO_3^- \tag{4}$$

$$HCO_3^- \rightarrow H^+ + CO_3^{2-} \tag{5}$$

$$2H^+ + 2e \rightarrow H_2 \tag{6}$$

The total reaction equation is:

$$Fe + CO_2 + H_2O \rightarrow FeCO_3 + H_2 \tag{7}$$

$$Fe + 2CO_2 + 2H_2O \rightarrow Fe(HCO_3)_2 + H_2 \tag{8}$$

(2) Reaction under the action of O_2:

$$4Fe + O_2 + H_2O \rightarrow 4Fe(OH)_2 \tag{9}$$

$$4Fe(OH)_2 + O_2 + 2H_2O \rightarrow 4Fe(OH)_3 \tag{10}$$

$$2Fe(OH)_3 \rightarrow Fe_2O_3 + 3H_2O \tag{11}$$

$$6FeO + O_2 \rightarrow Fe_3O_4 \tag{12}$$

(3) Reaction under the joint action of O_2 and CO_2:

$$4FeCO_3 + O_2 + 4H_2O \rightarrow 2Fe_2O_3 + 4H_2CO_3 \tag{13}$$

$$3FeO + CO_2 \rightarrow Fe_3O_4 + CO \tag{14}$$

The difference in corrosion product film composition can be obtained by comparing the single O_2/CO_2 environment and the coexistence of O_2 and CO_2. The corrosion products under a single O_2 environment are dominated by iron oxides (Fe_2O_3, Fe_3O_4). O_2 and CO_2 coexistence environments both exist. Combined with the corrosion morphology analysis, O_2 and CO_2 synergistic effect of oxygen corrosion and CO_2 corrosion characteristics. When the O_2 partial pressure increases, iron oxide production increases. But the corrosion product film is unstable and easy to peel off from the material's surface. J55 steel constantly undergoes CO_2 corrosion damage to the material. When J55 steel was in a lower oxygen concentration and CO_2 concentration, corrosion began to tend to exhibit characteristic CO_2 corrosion. And because $FeCO_3$ is more stable, it can effectively prevent dissolved oxygen penetration into the corrosion layer and aggravating corrosion.

3.3 Three-Dimensional Morphological Analysis after Removal of Corrosion Products

Fig. 8 shows the three-dimensional surface morphology of the hanging sheet under different corrosive media after the removal of corrosion products. Figs. 8a and 8c show that the J55 steel in a single O_2 environment and O_2/CO_2 coexistent environment both show different degrees of pitting corrosion. The pitting corrosion of J55 steel in the O_2/CO_2 coexistence environment is relatively more serious. There are more pitting areas and a greater degree of corrosion. The J55 steel in the single O_2 environment also had more pitting areas and the second highest degree of pitting corrosion. Fig. 8b shows that the corrosion area under a single CO_2 environment is larger, but the overall corrosion depth is smaller, indicating uniform corrosion.

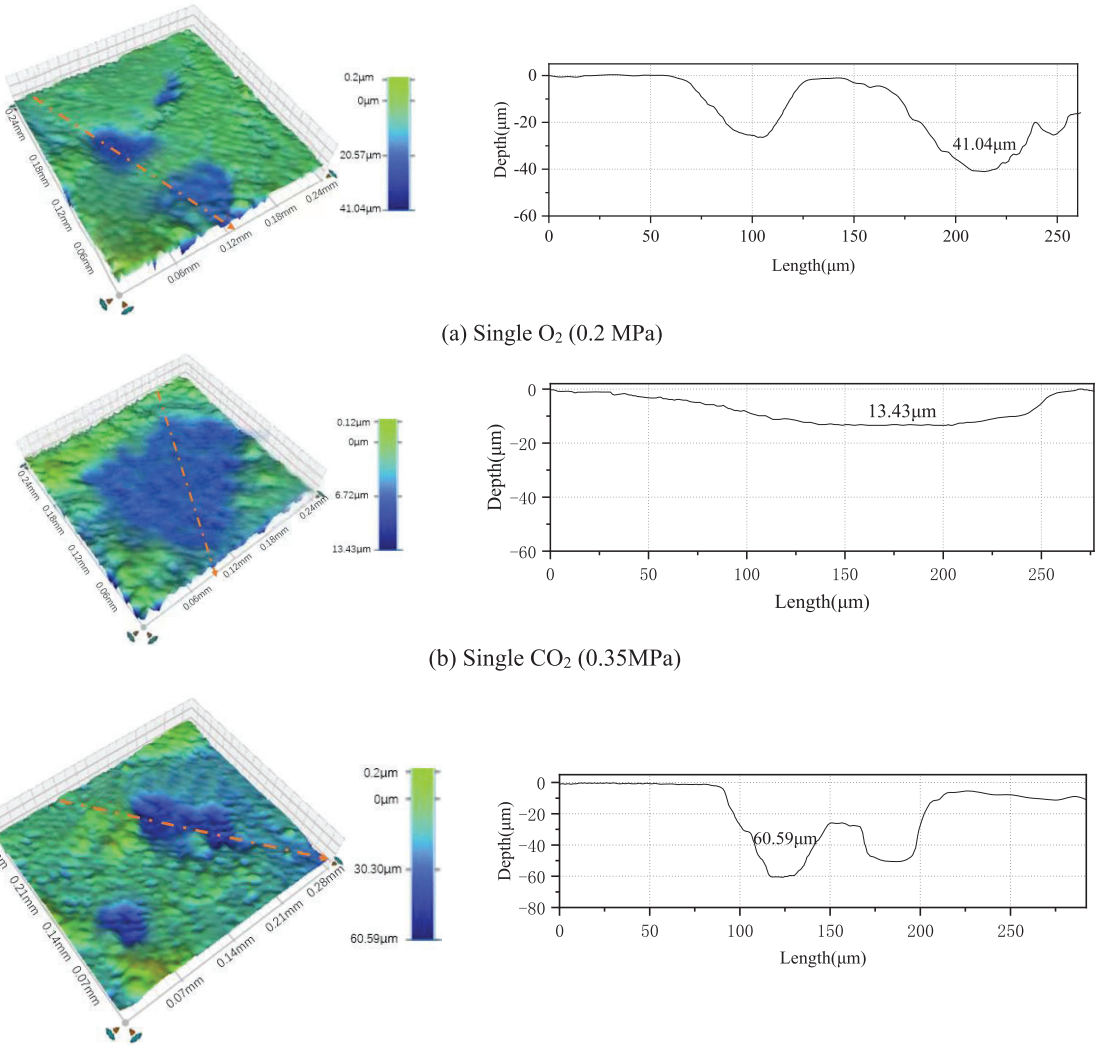

Figure 8: J55 steel in different corrosive media three-dimensional morphology and cross-sectional corrosion depth

The local corrosion pit depth and local corrosion rate of steel under the three corrosive media are shown in Table 4. The local corrosion rate under single O_2, single CO_2, and O_2/CO_2 coexistence environment are 2.14 mm/a, 0.70 mm/a, and 3.16 mm/a, respectively. The local corrosion rate under the O_2/CO_2 coexistence environment exceeds the sum of the local corrosion rate under a single O_2 environment and a single CO_2 environment. It means that when O_2 and CO_2 coexist, CO_2 accumulates on the surface of J55 steel, where pitting corrosion occurs, to further increase the depth of pitting corrosion. The presence of CO_2 aggravates the pitting corrosion of J55 steel.

Table 4: Maximum corrosion-depth measurement results of J55 steel under different corrosive media

Corrosive medium	0.2 MPa O_2	0.35 MPa CO_2	0.2 MPa O_2, 0.35 MPa CO_2
Maximum pitting pit depth/μm	41.04	13.43	60.59
Local corrosion rate/mm·a^{-1}	2.14	0.70	3.16

3.4 Analysis of the Rate of Corrosion of J55 Steel in Different Corrosive Media

The local rate of corrosion and average rate of corrosion of J55 steel in different corrosive media are shown in Fig. 9. Fig. 9 shows a single O_2 environment, corrosion products, and oxygen diffusion on the substrate with the increase in O_2 partial pressure. At the same time, the oxidation products are loose and porous, providing a channel for the corrosion medium, resulting in a gradual increase in the rate of corrosion of the material. And in a single CO_2 environment, the H+ content of the solution increases with the rise of CO_2 partial pressure, and the corrosion rate also increases.

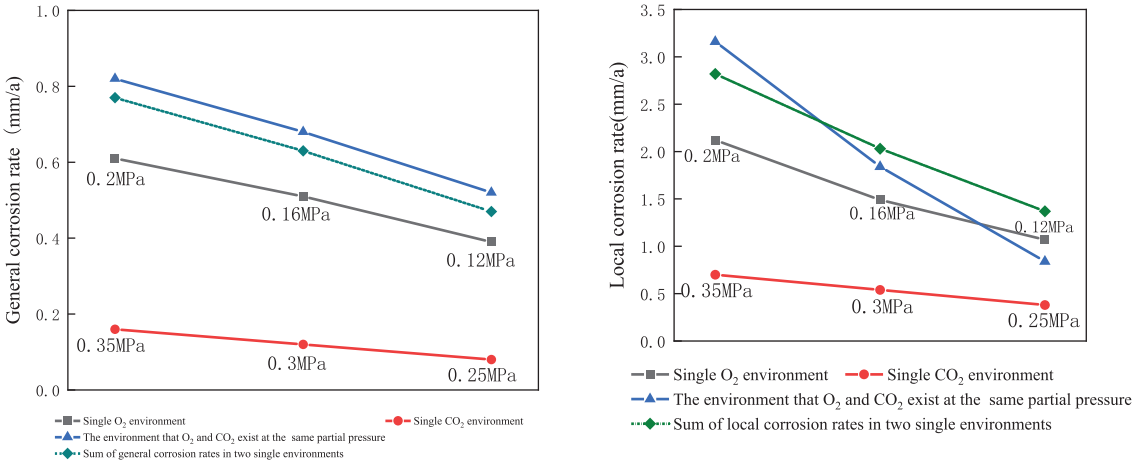

(a) uniform corrosion rate (b) local corrosion rate

Figure 9: J55 steel in different corrosive media under the uniform corrosion rate and local corrosion rate

The three sets of O_2/CO_2 coexistence environments correspond to the gas environment of the extraction well after injection of 10%, 8%, and 6% oxygen-reduced air, respectively. As seen in Fig. 9a, the sum of the uniform corrosion rate of a single O_2 environment and CO_2 environment is compared with the consistent corrosion rate of the O_2 and CO_2 coexistence environment under the same partial pressure. O_2 and CO_2 coexistence environments were found to have a significant synergistic effect on the overall corrosion of J55 steel.

As seen in Fig. 9b, the coexistence of O_2 and CO_2 gradually changes from promoting pitting to inhibiting pitting as the degree of oxygen-reduced air flooding increases. Combined with the microscopic morphology and XRD patterns, it is observed that the $FeCO_3$ crystals are finer and shift toward iron oxides when the oxygen concentration is higher. With the increased degree of oxygen-reduction, $FeCO_3$ can form a denser corrosion product film on the material surface. This can significantly weaken the synergistic pitting effect of O_2 and CO_2, reducing the risk of pitting and perforation of J55 steel pipes.

4 Conclusions

(1) When the oxygen concentration of 10% oxygen-reducing air is injected, the oxygen concentration and CO_2 concentration in the extraction well are high. It mainly shows the characteristics of oxygen corrosion, generating a large amount of iron oxide and a small amount of ferrous carbonate. As the oxygen-reducing air flooding increases, the oxygen concentration and CO_2 concentration in the extraction well decrease simultaneously, gradually showing the characteristics of CO_2 corrosion. A small number of iron oxides accompany the main corrosion product of ferrous carbonate.

(2) In the extraction well fluid medium, the environment contains both O_2 and CO_2, and the uniform corrosion rate is greater than the sum of the uniform corrosion rate in a single O_2 and a single

CO_2 environment at the same partial pressure. Thus, the synergistic effect of O_2 and CO_2 accelerates the overall corrosion of J55 steel.

(3) When O_2 and CO_2 coexist, CO_2 accumulates on the surface of J55 steel at the site of pitting corrosion and increases the pitting further. The accumulation of CO_2 at the pitting site will aggravate the pitting corrosion of J55 steel. The local corrosion rate of J55 steel in oxygen-reduced air with 6% oxygen concentration decreased by 2.32 mm/a compared with that in oxygen-reduced air with 10% oxygen concentration. This demonstrates that oxygen-reducing has an obvious effect of inhibiting pitting corrosion.

(4) As long as the cost of oxygen reduction allows, the degree of oxygen reduction of oxygen-reducing air drive is increased to 6%, which can guarantee the safety of the gas injection process. Moreover, the corrosion of J55 steel is significantly reduced, but corrosion protection measures such as corrosion inhibitors or anti-corrosion coatings are still needed to meet the site corrosion protection needs.

Funding Statement: Major national science and technology projects "Key Techniques for the Development of Low Abundance Tight Low Permeability Reservoirs" (2016ZX05048).

Conflicts of Interest: The authors declare that they have no conflicts of interest to report regarding the present study.

References

1. Moore, R. G., Mehta, S. A., Ursenbach, M. G. (2002). A guide to high pressure air injection (HPAI) based oil recovery. *SPE/DOE Improved Oil Recovery Symposium*, SPE-75207-MS. Tulsa, Oklahoma.
2. Liao, G., Wang, H., Wang, Z., Tang, J., Wang, B. et al. (2020). Oil oxidation in the whole temperature regions during oil reservoir air injection and development methods. *Petroleum Exploration and Development, 47(2),* 357–364. https://doi.org/10.1016/S1876-3804(20)60052-0
3. Ji, Y., Zhou, L., Zhao, Z. (2027). Risk analysis and safety control technology of air injection oil recovery process. *Petrochemical Safety and Environmental Protection Technology, 23(3),* 19–22.
4. Ren, S. (2016). Study on mixing and explosion propagation laws of natural gas in confined space. *Journal of Safety Science and Technology, 12(11),* 130–135.
5. Dong, B., Zeng, D., Yu, Z., Cai, L., Yu, H. et al. (2021). Major corrosion influence factors analysis in the production well of CO_2 flooding and the optimization of relative anti-corrosion measures. *Journal of Petroleum Science and Engineering, 200,* 108052. https://doi.org/10.1016/j.petrol.2020.108052
6. Zeng, D., Dong, B., Zeng, F., Yu, Z., Zeng, W. et al. (2021). Analysis of corrosion failure and materials selection for CO_2-H_2S gas well. *Journal of Natural Gas Science and Engineering, 86,* 103734. https://doi.org/10.1016/j.jngse.2020.103734
7. Huang, T., Ma, F., Fan, D., Liu, F., Zhao, M. (2020). Study on oxygen corrosion behavior of N80 casing steel by partial pressure ratio of CO_2 and O_2. *Petroleum Knowledge, 12(2),* 58–59.
8. Zhu, C., Liu, G., Dong, S., Li, X., Dong, B. et al. (2019). Effect of temperature on the corrosion of 3Cr steel in CO_2-O_2 environment species. *Journal of Iron and Steel Research, 31(6),* 573–581.
9. Zhang, J., Lin, X., Lu, S., Wang, T., Liu, W. et al. (2013). Corrosion behavior and mechanism of N80 steel under high temperature CO_2-O_2 coexisting condition. *Corrosion 2013,* 1121–1130, Orlando, Florida.
10. Zhang, S., Hou, L., Du, H., Wei, H., Liu, B. et al. (2020). A study on the interaction between chloride ions and CO_2 towards carbon steel corrosion. *Corrosion Science, 167,* 108531. https://doi.org/10.1016/j.corsci.2020.108531
11. Zhang, S., Li, Y., Liu, B., Mou, L., Yu, S. et al. (2022). Understanding the synergistic effect of CO_2, H_2S and fluid flow towards carbon steel corrosion. *Vacuum, 196,* 110790. https://doi.org/10.1016/j.vacuum.2021.110790
12. Raman, A. (1996). Reviews on corrosion inhibitor science and technology. *89 symposium*.
13. Wei, B. (1984). *Theory and application of corrosion of metals*, pp. 264–266. Beijing, China: Chemical Industry Press.

14. Wang, J., Lai, X., Wang, Q., Gao, H., Sun, Y. et al. (2007). Experimental study on oil drive by air injection in Zhongyuan oilfield. *Petroleum Drilling Technology, 35(2),* 5–7.
15. Zhou, Q. (2009). *Research on corrosion and corrosion protection of pipe column in air injection oil drive process (Ph.D. Thesis)*. China University of Petroleum, Qingdao.
16. Xie, T., Lin, H., Xu, J., Dou, P., Chen, Y. et al. (2017). CO_2 corrosion behavior of different materials of oil casing steel. *Surface Technology, 46(1),* 211–217.
17. Kermani, M. B., Morshed, A. (2003). Carbon dioxide corrosion in oil and gas production a compendium. *Corrosion, 59(8)*. https://doi.org/10.5006/1.3277596
18. Wang, N., Lu, Z., Shi, X. (2013). Oxygen corrosion prevention and control technology in tahe oilfield. *Surface Corrosion Control, 27(8),* 48–50.
19. Zhang, X., Liu, J., Yi, Y., Liu, W., Sun, L. (2006). Challenges and development of Gas injection recovery enhancement technology–Air injection low temperature oxidation technology. *Special Oil and Gas Reservoirs, 13(1),* 6–9.
20. Yu, Z., Zeng, D., Lin, Y., Zeng, G., Feng, Y. et al. (2020). Investigations on the oxygen corrosion behaviors of p110 steel in a dynamic experiment simulating nitrogen injection. *Materials and Corrosion, 71(8),* 1375–1385. https://doi.org/10.1002/maco.202011490
21. Sun, Y., Fu, C., Yang, X. (2012). Corrosion analysis of oil pipe in injection exploitation of high temperature multicomponent thermal fluid. *Chemical Engineering of Oil & Gas, 41(4),* 408–410.
22. Wang, L., Hu, R., Wang, X. H. (2006). The oxygen corrosion behavior of S135 drill pipe steel in drill fluid. *Petroleum Machinery, 34(10),* 1–4.
23. Lin, X., Liu, W., Zhang, J., Dong, S., Zhang, H. et al. (2013). Characteristics of corrosion scale of 3Cr steel at high temperature and pressure in an O_2 and CO_2 environment. *Acta Physico-Chimica Sinica, 29(11),* 2405–2414. https://doi.org/10.3866/PKU.WHXB201309171
24. Li, X. (2018). Experimental study on oxygen corrosion law and protection of downhole string in air injection process. *Science Technology and Engineering, 18,* 18–25.
25. Khalaj, G., Pouraliakbar, H., Arab, N., Nazerfakhari, M. (2015). Correlation of passivation current density and potential by using chemical composition and corrosion cell characteristics in HSLA steels. *Measurement, 75,* 5–11. https://doi.org/10.1016/j.measurement.2015.07.048
26. Khalaj, G., Khalaj, M. J. (2016). Investigating the corrosion of the heat-affected zones (HAZs) of API-x70 pipeline steels in aerated carbonate solution by electrochemical methods. *International Journal of Pressure Vessels and Piping, 145,* 1–12. https://doi.org/10.1016/j.ijpvp.2016.06.001
27. Kiahosseini, S. R., Mohammadi Baygi, S. J., Khalaj, G., Khoshakhlagh, A., Samadipour, R. (2018). A study on structural, corrosion, and sensitization behavior of ultrafine and coarse grain 316 stainless steel processed by multiaxial forging and heat treatment. *Journal of Materials Engineering and Performance, 27(1),* 271–281. https://doi.org/10.1007/s11665-017-3095-7
28. Boga, H. I., Ludwig, W., Brune, A. (2003). Sporomusa aerivorans sp. nov., an oxygen-reducing homoacetogenic bacterium from the gut of a soil-feeding termite. *International Journal of Systematic and Evolutionary Microbiology, 53(5),* 1397–1404. https://doi.org/10.1099/ijs.0.02534-0